Supplementary Information for 'Asymptotic Analysis of Subglacial Plumes in Stratified Environments' by Bradley et al.

Alexander T Bradley, C. Rosie Williams,
Adrian Jenkins, Robert Arthern

In this supplementary information we provides further details on the analysis presented in the main text. This supplementary consists of five sections: in the first, we explicitly state the solution in region one and associated matching conditions for region two; in the second, we explicitly state the pycnocline-rescaled plume model equations; in the third, we provide details of the behaviour of solutions in region three in the limit $X \to X_c$; in the fourth section we provide further details of the behaviour in region 4; finally, we describe our construction of an approximation to the melt rate, which builds upon the asymptotic analysis presented in §3 of the main text.

1 Solution for Region One and Matching Conditions on Region Two

The solution to the leading order equations appropriate for region one, given by (3.1)–(3.4) in the main text, is:

$$U(X) = \left(\frac{2\kappa}{3}\right)^{1/2} \left[Z_b'(X)\right]^{1/3} \left[1 - Z_b(X)\right]^{1/3} I(X)^{1/2}, \tag{1}$$

$$D(X) = \frac{2}{3} \left[Z_b'(X)\right]^{-1/3} \left[1 - Z_b(X)\right]^{-1/3} I(X), \tag{2}$$

$$\Delta\rho(X) = \kappa \left[1 - Z_b(X)\right], \tag{3}$$

$$\Delta T = \left[1 - Z_b(X)\right] Z_b'(X) - \frac{2}{3} \left[Z_b'(X)\right]^{2/3} \left[1 - Z_b(X)\right]^{-1/3} I(X), \tag{4}$$

where

$$I(X) = \int_0^X \left[Z_b'(\xi)\right]^{4/3} \left[1 - Z_b(\xi)\right]^{1/3} \, \mathrm{d}\xi. \tag{5}$$

The matching conditions on region two are therefore given by

$$U \to U_{\text{in}} = \left(\frac{2\kappa}{3}\right)^{1/2} \left[Z_b'(X_p)\right]^{1/3} \left[1 - Z_b(X_p)\right]^{1/3} I(X_p)^{1/2}, \tag{6}$$

$$D \to D_{\text{in}} = \frac{2}{3} \left[Z_b'(X_p)\right]^{-1/3} \left[1 - Z_b(X_p)\right]^{-1/3} I(X_p), \tag{7}$$

$$\Delta\rho \to \Delta\rho_{\text{in}} = \kappa \left[1 - Z_b(X_p)\right], \tag{8}$$

$$\Delta T \to \Delta T_{\text{in}} = \left[1 - Z_b(X_p)\right] Z_b'(X_p) - \frac{2}{3} \left[Z_b'(X_p)\right]^{2/3} \left[1 - Z_b(X_p)\right]^{-1/3} I(X), \tag{9}$$

as $\zeta = (X - X_p)/\delta \to -\infty$.

2 Pycnocline-rescaled plume model equations

The pycnocline-rescaled plume model equations referred to in §3.2 in the main text read:

$$\frac{\mathrm{d}(DU)}{\mathrm{d}\zeta} = \delta U Z_b'(X_p + \delta\zeta) + k_3 \epsilon_1 \delta U \Delta T, \tag{10}$$

$$c_1 \frac{\mathrm{d}(DU^2)}{\mathrm{d}\zeta} = D\Delta\rho Z_b'(X_p + \delta\zeta) - U^2, \tag{11}$$

$$\frac{\mathrm{d}(DU\Delta\rho)}{\mathrm{d}\zeta} = -P_B \operatorname{sech}^2(\zeta) Z_b'(X_p + \delta\zeta) DU + \delta \left[\kappa - k_4 \epsilon_1 \tanh(\zeta)\right] U\Delta T \tag{12}$$

$$c_2 \frac{\mathrm{d}(DU\Delta T)}{\mathrm{d}\zeta} = \left\{1 - Z_b(X_p + \delta\zeta) - P_T \left[1 + \tanh(\zeta)\right] - D\right\} U Z_b'(X_p + \delta\zeta) - U\Delta T. \tag{13}$$

3 Analysis of Region Three in the Limit $X \to X_c$

In this section, we describe the behaviour of solutions of the leading order equations for region three in the limit $X \to X_c$, where the velocity U approaches zero. Recall that these leading order equations are

$$(DU)' = U Z_b', \tag{14}$$

$$0 = D\Delta\rho Z_b' - U^2, \tag{15}$$

$$(DU\Delta\rho)' = \kappa U \Delta T \tag{16}$$

$$0 = (1 - 2P_T - Z_b) Z_b' U - U\Delta T - DU Z_b', \tag{17}$$

and that the flux $Q = DU$ evolves according to

$$\frac{\left[Q'(X)\right]^3}{\left[Z_b'(X)\right]^4} = \kappa \left\{\left[1 - Z_b(X) - 2P_T\right] Q(X) - \left[1 - Z_b(X_p) - 2P_T\right] Q_{\text{in}}\right\} + \frac{U_{\text{out}}^3}{Z_b'(X_p)}. \tag{18}$$

The point X_c satisfies

$$[1 - Z_b(X_c)]\,Q_c - 2P_T\,(Q_c - Q_{\text{in}}) - \left[1 - Z_b(X_p)\right] Q_{\text{in}} + \frac{U_{\text{out}}^3}{\kappa Z_b'(X_p)} = 0. \tag{19}$$

where $Q_c = Q(X_c)$.

Since the velocity $U \to 0$ as $X = X_c$, we must introduce rescaled variables to reflect a change in asymptotic order; we therefore introduce

$$X = X_c + \varepsilon \tilde{X}, \quad Q = Q_c + \varepsilon^\gamma \tilde{Q} \tag{20}$$

where $\varepsilon \ll 1$ is arbitrary, $\tilde{X} = O(1)$ is negative, $\tilde{Q} = O(1)$ and $\gamma > 0$ is to be determined. Inserting (20) into (18) gives

$$\varepsilon^{3(\gamma-1)} \frac{(\tilde{Q}')^3}{\left[Z_b'(X_c)\right]^4}\,[1 + O(\varepsilon)] = -\varepsilon\lambda\tilde{X} Z_b'(X_c) Q_c + \\ \varepsilon^\gamma\,[1 - 2P_T - Z_b(X_c)]\,\tilde{Q} + O(\varepsilon^2, \varepsilon^{\gamma+1}). \tag{21}$$

A dominant balance is obtained in (21) by taking $\gamma = 4/3$. After setting $\gamma = 4/3$ in (21), using $Q' = UZ_b'$ [from (14)] and undoing the rescaling (20), we find

$$U \sim \kappa^{1/3} Z_b'(X_c)^{2/3} Q_c^{1/3} (X_c - X)^{1/3} \quad \text{as } X \to X_c^-. \tag{22}$$

From (20), we have $Q \sim Q_c + O(\varepsilon^{4/3})$. Combining this with (14) gives

$$D \sim \kappa^{-1/3} Z_b'(X_c)^{-2/3} Q_c^{2/3} (X_c - X)^{-1/3} \quad \text{as } X \to X_c^-. \tag{23}$$

A balance in the momentum equation (15) gives

$$\Delta\rho \sim \kappa Z_b'(X_c)(X_c - X) \quad \text{as } X \to X_c^-, \tag{24}$$

while a balance in the thermal driving equation (17) requires

$$\Delta T \sim -\kappa^{-1/3} Z_b'(X_c)^{1/3} Q_c^{2/3} (X_c - X)^{-1/3} \quad \text{as } X \to X_c^-. \tag{25}$$

4 Further Details of Region Four Behaviour

In this section, we provide further details of the behaviour of the leading order equations in region four. Recall that these equations are

$$\frac{\mathrm{d}(\mathcal{D}\mathcal{U})}{\mathrm{d}\chi} = 0, \qquad \frac{\mathrm{d}(\mathcal{D}\mathcal{U}^2)}{\mathrm{d}\chi} = \mathcal{D}\Delta\varrho Z_b'(X_c) - \mathcal{U}^2, \tag{26}$$

$$\frac{\mathrm{d}(\mathcal{D}\mathcal{U}\Delta\varrho)}{\mathrm{d}\chi} = \kappa\mathcal{U}\Delta\mathcal{T}, \qquad k_2 \frac{\mathrm{d}(\mathcal{D}\mathcal{U}\Delta\mathcal{T})}{\mathrm{d}\chi} = -\mathcal{U}\Delta\mathcal{T} - \mathcal{D}\mathcal{U}Z_b'(X_c). \tag{27}$$

for $\chi > -\infty$. Equations (26)–(27) must satisfy the matching conditions

$$\mathcal{U} \sim \kappa^{1/3} Z_b'(X_c)^{-2/3} Q_c^{1/3} (-\chi)^{1/3}, \qquad \mathcal{D} \sim \kappa^{-1/3} Z_b'(X_c)^{-2/3} Q_c^{2/3} (-\chi)^{-1/3}, \tag{28}$$

$$\Delta\varrho \sim -\kappa Z_b'(X_c)\chi, \qquad \Delta\mathcal{T} \sim -\kappa^{-1/3} Z_b'(X_c)^{1/3} Q_c^{2/3} (-\chi)^{-1/3}. \tag{29}$$

We begin by nothing that from the first of (26), flux is conserved, i.e.

$$\mathcal{D}\mathcal{U} = Q_c. \tag{30}$$

Also, after inserting (30) into the second of (27), we obtain an expression that can be directly integrated to give

$$\frac{\Delta\varrho}{\kappa} + k_2 \Delta\mathcal{T} = -Z_b'(X_c) + C, \tag{31}$$

where C is a constant that would be determined by analysing the higher order contributions to $\Delta\rho$ as $X \to X_c$. This higher order analysis is beyond the scope of this paper.

The relationships (30) and (31) allow us to reduce (26)–(27) to a system of two equations, which can be rescaled so that only a single parameter, k_2, enters:

$$\tilde{\mathcal{U}} \frac{\mathrm{d}\tilde{\mathcal{U}}}{\mathrm{d}\tilde{\chi}} = \tilde{\Delta\varrho} - \tilde{\mathcal{U}}^3, \qquad k_2 \frac{\mathrm{d}\tilde{\Delta\varrho}}{\mathrm{d}\tilde{\chi}} = -\tilde{\mathcal{U}}\left[\tilde{p} + \tilde{\chi}\right], \tag{32}$$

where

$$\tilde{\chi} = \frac{\kappa^{1/4} Z_b'(X_c)^{1/2}}{Q_c^{1/2}} \left(\chi - \frac{C}{\kappa Z_b'(X_c)}\right), \tag{33}$$

$$\tilde{\mathcal{U}} = \frac{1}{\kappa^{1/4} Z_b'(X_c)^{1/2} Q_c^{1/2}} \mathcal{U}, \tag{34}$$

$$\tilde{\Delta\varrho} = \frac{1}{\kappa^{3/4} Z_b'(X_c)^{1/2} Q_c^{1/2}} \Delta\varrho. \tag{35}$$

In terms of these rescaled variables, the matching conditions (28)–(29) read

$$\tilde{\Delta\varrho} \sim -\tilde{\chi}, \; \tilde{\mathcal{U}} \sim (-\tilde{\chi})^{1/3} \quad \text{as } \tilde{\chi} \to -\infty. \tag{36}$$

The system (32)–(36) must be solved numerically. In figure 1, we present a comparison between numerical solutions of equations (32) and the solutions of the full equations [model equations (2.30)–(2.33) in the main text rescaled according to (3.31)–(3.32)]. We see good agreement, with solutions predominantly following the nullcline $\tilde{\Delta\varrho} = \tilde{\mathcal{U}}^3$, before deviating when the rescaled buoyancy deficit $\tilde{\Delta\varrho}$ approaches zero. Eventually, the buoyancy deficit goes negative, indicating that the plume has become negatively buoyant; the plume's upward motion continues for a short distance owing to inertia, before ultimately reaching $\tilde{\mathcal{U}} = 0$, where it terminates. For the purpose of constructing an approximation to the melt rate, it is worth noting that the rescaled buoyancy is approximately linear (figure 1b); using this, the nullcline solution for $\tilde{\mathcal{U}}$, which holds nearly everywhere in this region, can be approximated by $\tilde{\mathcal{U}} = \tilde{\chi}^{1/3}$. After undoing the rescaling (33)–(35), this approximate solution reduces to equation (3.37) in the main text.

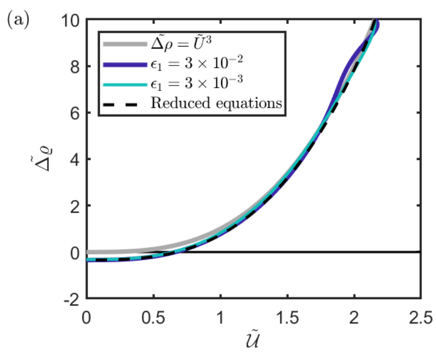

Figure 1: Numerical solutions of original model equations [(2.30)–(2.33) in the main text] rescaled according to (3.31)–(3.32) and with $\epsilon_1 = 3 \times 10^{-2}$ (i.e. as in table 2 of the main text, purple curves) and with $\epsilon_1 = 3 \times 10^{-3}$ (cyan curves) which are shown in (a) $(\tilde{\mathcal{U}}, \tilde{\Delta\varrho})$ space and (b) $(\tilde{\chi}, \tilde{\Delta\varrho})$ space [$\tilde{\chi}$, $\tilde{\mathcal{U}}$, and $\tilde{\Delta\varrho}$ are a spatial variable, plume velocity, and buoyancy deficit, respectively, and are defined in (33)–(35)]. The black dashed curve indicates the numerical solution of the reduced equations (32), and the grey curve indicates the nullcline $\tilde{\mathcal{U}}^3 = \tilde{\Delta\varrho}$. The solid black line indicates $\tilde{p} = 0$. Each of the solutions here uses a linear draft, $Z_b(X) = X$, with $Q_c = 0.5$, $X_c = 0.5$ and κ, k_i according to the values in table 2 of the main text. The matching conditions (28)–(29) are applied at $\tilde{\chi}_0 = 10$ in both cases, i.e. the solution domain shown is $-\tilde{\chi}_0 < \tilde{\chi} < \tilde{\chi}_t$, where $\tilde{\chi}_t$ is the value of $\tilde{\chi}$ at which the plume velocity reaches zero.

5 Melt Rate Construction

In this section, we describe our analytic approximation $M_p(X)$ to the melt rate $M(X) = U(X)\Delta T(X)$ that emerges from the model equations (2.30)-(2.33) in the main text. This approximation builds upon the asymptotic analysis of §3 of the main text, and we consider each of the four regions identified therein in turn.

5.1 Region one

Recall that in region one, the solution to the leading order equations can be expressed analytically; our approximation M_p therefore takes values specified by the corresponding leading order contribution to $U\Delta T$:

$$M_p = M_{p,1}(X) = \left(\frac{2\kappa}{3}\right)^{1/2} Z_b'(X)\,[I(X)]^{1/2}\left\{[1 - Z_b(X)]^{1/3}\left[Z_b'(X)\right]^{1/3} - \frac{2}{3}I(X)\right\} \quad (37)$$

where $I(X)$ is given in equation (3.5) of the main text. The approximation (37) is valid for $0 < X < X_p - N_l\delta$, where $N_l = O(1)$ is introduced to account for the finite extent of the pycnocline: we define the pycnocline region in the approximation constructed here as $X_p - N_l\delta < X < X_p + N_l\delta$, i.e. the quantity $2N_l$ describes the number of (dimensionless) pycnocline length scales required for the solution to transition between the constant values of the velocity and thermal driving on either side of the pycnocline. We must make a choice for N_l; in what follows we take $N_l = 2$, a choice that is informed by the solutions of equations (3.8)-(3.11) in the main text, which are shown in figure 4 of the main text. There it can be seen that the majority of the rapid change close to the centre of the pycnocline occurs over a length bounded by four dimensionless pycnocline length scales (the light blue boxes in figure 4 of the main text have height 4δ, when measured in terms of the outer variable X). The results presented here are insensitive to the value of N_l, provided that it is not too large: for $N_l \gtrsim 4$, the pycnocline region takes up a disproportionately large portion of the water column, resulting in large errors not only in this region, but also in those regions above it, which rely on the solution in the pycnocline region.

The integrals in (37) must be evaluated numerically in general, but accurate analytic approximations are readily computed provided that the ice shelf basal geometry is known. In the case that the ice shelf base has a constant slope, the approximation (37) reduces to the solution described by Lazeroms et al. [1]:

$$M_{\mathrm{L19}}(X) = \frac{\kappa^{1/2}}{2\sqrt{2}}\left[1 - (1 - X)^{4/3}\right]^{1/2}\left[3(1 - X)^{4/3} - 1\right]. \quad (38)$$

We refer to the dimensional form of (38) as the 'L19 approximation' in the main text.

Lazeroms et al. [1] also describe an ad-hoc method designed to account for non-constant basal slopes, in which all factors of the aspect ratio in the L19 approximation are replaced by the local slope of the ice shelf base, and is equivalent to multiplying (38) by a factor of $Z_b'(X)^{3/2}$; the corresponding approximation to the melt rate is

$$M_{\mathrm{L19AH}}(X) = \frac{\kappa^{1/2}}{2\sqrt{2}}\left[Z_b'(X)\right]^{3/2}\left[1-(1-X)^{4/3}\right]^{1/2}\left[3(1-X)^{4/3}-1\right]. \tag{39}$$

The dimensional form of (39) is referred to as the 'L19AH approximation' henceforth. Lazeroms et al. [1] demonstrated that, and we show in §4 of the main text, that this simple method is reasonably effective at accounting for a non-constant basal slope.

The two-dimensional extensions of the L19 (38) and L19AH (39) approximations represent the current state of the art in plume-physics based melt rate parametrizations and therefore act as a benchmark against which the approximation constructed in this section is assessed (see §4 of the main text).

5.2 Region two

Unlike in region one, the leading order equations for region two [(3.8)-(3.11) in the main text] do not have an analytic solution. We therefore construct our approximation based on expressions (3.19) and (3.21) in the main text for the change in U and ΔT across a relatively slender pycnocline: we linearly interpolate according to these values, giving

$$\begin{aligned} M_p = M_{p,2}(X) &\coloneqq \\ &\left[U_{\mathrm{out}} + [U]_{\mathrm{pyc}}\frac{X-(X_p+N_l\delta)}{2N_l\delta}\right]\left[\Delta T_{\mathrm{out}} + [\Delta T]_{\mathrm{pyc}}\frac{X-(X_p+N_l\delta)}{2N_l\delta}\right], \end{aligned} \tag{40}$$

for $X_p - N_l\delta < X < X_p + N_l\delta$. [Recall that U_{out}, $[U]_{\mathrm{pyc}}$, ΔT_{out}, and $[\Delta T]_{\mathrm{pyc}}$ are set out explicitly in equations (3.18), (3.19), (3.22), and (3.23) of the main text, respectively.] Although the situation is not expected for parameter values appropriate for Antarctica [as discussed in §3 of the main text], in the case that $\Delta\rho_{\mathrm{out}} < 0$, we apply (40) only as far as $M_{p,2} = 0$ and take $M_p = 0$ downstream of this point.

5.3 Region three

Extra care must be taken for region three, owing to the dearth of information about the leading order solution in this region: our knowledge is limited to understanding that the velocity decreases until it reaches zero at an a priori unknown point X_c, and a description of the behaviour of solutions close to X_c [in particular, we showed that $U \sim (X_c - X)^{1/3}$ as $X \to X_c$]. In this section, we describe a way to construct an appropriate approximation to the melt rate which exploits the information available, but stress that we make several ad hoc choices, and the construction presented below is by no means unique.

Our strategy for this region, $X_p + 2N_l\delta < X < X_c$, is to split it into two further regions: a lower part, $X_p + 2N_l < X \leq X^*$, and an upper, part $X^* < X < X_c$. We choose to take X^* to be smaller of X_{fr}, the value of X that corresponds to the ice shelf front, and the point at which the velocity has decayed to some fraction $0 < f < 1$ of U_{out}, the velocity of the plume when it enters region three from below.

For the lower part, $X_p + 2N_l\delta < X \leq X^*$, we exploit the proximity to the pycnocline to artificially construct a small parameter, and seek an asymptotic expansion of the pertinent variables in this parameter. For the upper half, $X^* < X < X_c$, we mimic the behaviour as $X \to X_c$; in doing so we are able to simultaneously describe the behaviour in this region whilst also determining the values of X_c and $Q_c = Q(X_c)$.

In more detail, for the lower half we introduce $\varepsilon = X^* - X_p$, which we shall assume to be a small, positive parameter. We verify *a posteriori*, once X^* has been determined as outlined below, that $\varepsilon \ll 1$. Note, however, that because the vertical lengthscale chosen in §2 of the main text is typically much larger than the grounding line depth, we expect to have $X_{\mathrm{fr}} < 1$ and thus $\varepsilon < 1$.

We then set $X = X_p + \varepsilon Y$, where $Y = O(1)$, in the ODE (18) for the flux Q in region three, and attempt to account for variations in Q away from $Q_{\mathrm{in}} = Q(X_p)$ by expanding in powers of ε:

$$Q = Q_{3l} \coloneqq Q_{\mathrm{in}} + \sum_{i=1}^{\infty} \varepsilon^i Q_i(Y), \qquad Q_i \sim O(1). \tag{41}$$

Equating powers of ε leads to a hierarchy of simple ODEs for the Q_i, which can be solved analytically in series. Solving the equations that arise at $O(1)$, $O(\varepsilon)$, and $O(\varepsilon^2)$ gives, respectively, $Q_1(Y) = K_1 Y, Q_2(Y) = K_2 Y^2, Q_3(Y) = K_3 Y^3$, where the K_i, $i = 1,\ 2,\ 3$ are known functions of κ, U_{out}, P_T, and Z_b.

Using $Q' = UZ_b'$ from before, the velocity associated with (41) is

$$U = U_{3l} \coloneqq \frac{1}{Z_b'(X)} \sum_{i=1}^{\infty} \varepsilon^{i-1} \frac{\mathrm{d}Q_i}{\mathrm{d}Y}. \tag{42}$$

We use (42) to determine X^*: by retaining only the first three terms in the expansion (42), and making the approximation $Z_b'(X) \approx Z_b'(X_p)$ (i.e. ignoring any variation in the ice shelf base in this region), we find that X^*, provided that it is less than X_{fr}, must satisfy the quadratic equation

$$fU_{\mathrm{out}} = \frac{1}{Z_b'(X_p)} \left[K_1 + 2K_2(X^* - X_p) + 3K_3(X^* - X_p)^2 \right]. \tag{43}$$

In what follows we take $f = 0.7$, i.e. X^* is the maximum of X_{fr} and the point at which the plume speed according to (42) drops to approximately 70% of U_{out}. In the case that (43) has no solution, we assume that the plume reaches the ice shelf front without terminating, taking $X^* = X_{\mathrm{fr}}$ and ignoring any further contributions to the melt rate. We verified that our constructed parametrization is insensitive to the choice of f, provided that both f and $(1 - f)$ remain $O(1)$, i.e. region three is not dominated by either the lower or upper part.

Having constructed an approximation to both the flux and velocity in the lower part of region three, we have the ingredients necessary to determine the thermal driving from (17) and thus an approximation to the melt rate. However, since the expansion (41) only accounts for the ice shelf geometry at $X = X_p$, we postulate that it will perform poorly when applied to ice shelves with significant geometric variations above the pycnocline. In lieu of an analytic method that accounts for non-constant basal slopes, we apply the same ad-hoc geometric dependence as Lazeroms et al. [2]. Our approximation to melt rate therefore takes values

$$M_p(X) = M_{p,3l}(X) := Z_b'(X)^{5/2}\left\{[1 - 2P_T - Z_b(X)]\, U_{3l}(X) - Q_{3l}(X)\right\} \tag{44}$$

for $X_p + N_l\delta < X < X^*$. [Explicitly, the prefactor $Z_b'(X)^{5/2}$ arises as the product of $Z_b'(X)$, which appears in the conservation of thermal driving (17), and $Z_b'(X)^{3/2}$, the scaling of the aspect ratio in the non-dimensionalization.]

Our construction in the upper part of region three, $X^* < X < X_c$, is motivated by the asymptotic behaviour as $X \to X_c$. Since Q_c, and thus the prefactor in (3.29) in the main text, are unknown, we first express the velocity in $X^* < X < X_c$ according to the asymptotic behaviour as $X \to X_c$ (3.26) albeit with an arbitrary prefactor:

$$U = U_{3u} = C(X_c - X)^{1/3}, \tag{45}$$

where C and X_c are to be determined. Note that since the solution in region four can be approximated by a solution of the form (45) [see §3d of this supplementary material], the below is also considered to be appropriate for region four.

After asserting that the velocity must be continuously differentiable across X^*, C and X_c are uniquely determined from (42) and (45) as

$$X_c = X^* + \frac{U_{3l}(X^*)}{3U_{3l}'(X^*)}, \qquad C = \frac{U_{3l}(X^*)}{(X_c - X^*)^{1/3}}. \tag{46}$$

In the case that this procedure gives $X_c < X^*$ [i.e. if $U_{3l}'(X_c) > 0$], we set $X^* = X_{\mathrm{fr}}$ and the upper part of region three is considered moot.

Our approximation to the melt rate in $X^* < X < X_c$ is then constructed using (17) and applying the ad-hoc geometric dependence:

$$M_p(X) = M_{p,3u}(X) := Z_b'(X)^{5/2}\left\{[1 - 2P_T - Z_b(X)]\, U_{3u}(X) - Q_{3l}(X^*)\right\} \tag{47}$$

for $X^* < X < X_c$. Note that in (47), we have made the approximation $Q \approx Q_{3l}(X^*)$ for all $X^* < X < X_c$, which is justified based on the fact that the flux is constant as $X \to X_c$ (see §2 of the supplementary information).

In summary, except for the special cases mentioned above, our approximation to the dimensionless melt rate takes values

$$M_p(X) = \begin{cases} M_{p,1}(X) & \text{[equation (37)]} \quad 0 < X \le X_p - N_l\delta, \\ M_{p,2}(X) & \text{[equation (40)]} \quad X_p - N_l\delta < X \le X_p + N_l\delta, \\ M_{p,3l}(X) & \text{[equation (44)]} \quad X_p + N_l\delta < X \le X^*, \\ M_{p,3u}(X) & \text{[equation (47)]} \quad X^* < X \le X_c. \end{cases} \tag{48}$$

The corresponding construction in the special cases are set out below.

Our approximation to the dimensional melt rate is obtained by undoing the various scalings:

$$\dot{m} = \left(\frac{\beta_S S_l g E_0^3 \alpha^3}{\lambda C_d (L/c)^3}\right)^{1/2} \tau^2 M_p\left(\frac{\lambda \alpha X}{\tau}\right), \tag{49}$$

where the X in the argument of M_p is dimensional. In the main text, we refer to (49) as the 'B22 approximation'.

The first special case arises when $\Delta\rho_{\text{in}} - 2P_B Z_b'(X_p) < 0$. Our analysis suggests that, in this case, the plume will intrude into the ambient within the pycnocline. Our constructed melt rate takes a linear interpolation across the pycnocline as in the approximation presented in the main text [equation (4.12) therein] that is modified to include zero speed and thermal driving upon exiting:

$$M_p = \begin{cases} M_{p,1} & \text{[equation (4.1)]} \quad 0 < X < X_p - N_l\delta, \\ M_{p,2} & \text{[equation (4.4)]} \quad X_p - N_l\delta < X < X_{\text{sep}}, \\ 0 & \qquad\qquad\qquad\quad\; X > X_{\text{sep}}, \end{cases} \tag{50}$$

where X_{sep} is the value of X at which $M_{p,2} = 0$. We note that the formulation (50) does not account for the subregion within the pycnocline in which the buoyancy deficit ceases to be $O(1)$ and the plume velocity reaches zero; this is justified on account of this region having a lengthscale which is $O(\epsilon_1\delta)$, meaning that it is unimportant on the lengthscale of the entire shelf.

The second exception case occurs when no physically relevant solution of (4.7), which describes the 'cross-over' point X^* must satisfy, exists. In this case, the scaled melt rate takes values

$$M_p = \begin{cases} M_{p,1} & \text{[equation (4.1)]} \quad 0 < X < X_p - N_l\delta, \\ M_{p,2} & \text{[equation (4.4)]} \quad X_p - N_l\delta < X < X_p + N_l\delta, \\ M_{p,3l} & \text{[equation (4.8)]} \quad X > X_p + N_l\delta. \end{cases} \tag{51}$$

Finally, if the computed termination point X_c does not satisfy $X_c > X^*$, we take M_p as in (51).

References

[1] Lazeroms WMJ, Jenkins A, Rienstra SW, Van De Wal RSW. An analytical derivation of ice-shelf basal melt based on the dynamics of meltwater plumes. J Phys Oceanogr. 2019;49(4):917-39.

[2] Lazeroms WMJ, Jenkins A, Gudmundsson H, van de Wal RSW. Modelling present-day basal melt rates for Antarctic ice shelves using a parametrization of buoyant meltwater plumes. Cryosphere. 2018;12(1):49-70.